Optogenetic control of microglia membrane potential reveals signal transduction in chemotaxis

Laura Laprell*, Christian Schulze, Marie-Luise Brehme and Thomas G. Oertner*

Institute for Synaptic Physiology, Center for Molecular Neurobiology Hamburg (ZMNH), University Medical Center Hamburg-Eppendorf, 20251 Hamburg, Germany

* Corresponding authors: laura.laprell@zmnh.uni-hamburg.de
thomas.oertner@zmnh.uni-hamburg.de

Summary

Microglia react to danger signals by rapid and targeted extension of cellular processes towards the source of the signal. This positive chemotactic response is accompanied by a hyperpolarization of the microglia membrane. Here we show that optogenetic depolarization of microglia has little effect on baseline motility, but significantly slows down the chemotactic response. Reducing the extracellular Ca^{2+} concentration mimics the effect of optogenetic depolarization. As the membrane potential sets the driving force for Ca^{2+} entry, hyperpolarization is an integral part of rapid stimulus-response coupling in microglia. Compared to other excitable cells, the sign of the activating response is inverted in microglia, leading to inhibition by depolarizing channelrhodopsins.

Introduction

Microglia – the only resident immune cells in the brain – are the first responders to external and internal threats in the central nervous system. They account for 5-10% of total brain cells and constantly surveil the brain parenchyma. Under physiological conditions microglia are highly ramified, have a small cell body and span approximately 50 µm in diameter. With their thin processes, microglia detect changes in the extracellular space, such as dying neurons, danger signals (e.g. adenine nucleotides), invading organisms, or alterations in neuronal activity (Nimmerjahn, 2005).

Under physiological conditions, THIK-1 and possibly TRP and chloride-conducting channels contribute to the resting membrane potential in microglia, which sits around -40 mV (Madry et al., 2018; Newell and Schlichter, 2005; Schilling and Eder, 2015). Deviations from this potential in both directions have been linked to microglia activation. Under pathological conditions, microglia exhibit two modes on how they change their membrane potential, (i) sustained hyperpolarization in chronically activated microglia and (ii) rapid, transient hyperpolarization induced by extracellular ATP in the vicinity of tissue damage. Sustained pathological hyperpolarization in activated and in aged microglia is correlated with an increased expression of Kir2.1 and Kv1.3 channels (Rangaraju et al., 2015; Schilling and Eder, 2015). This additional hyperpolarization is thought to be a precondition for the initiation of microglia functions, such as phagocytosis, chemotaxis and cytokine release, which are potentially promoted by the larger driving force for Ca^{2+} influx (Ince et al., 1988; Kouri et al., 1980; Paolicelli et al., 2011). While sustained hyperpolarization is accompanied by process retraction leading to an ameboid microglia morphology, transient hyperpolarization due to local tissue damage induces rapid process extension towards the source of extracellular ATP and Ca^{2+} transients in the processes directed towards the damage site (Eder, 2005; Lee et al., 2008; Nimmerjahn, 2005; Pozner et al., 2015). Detection of extracellular ATP and chemotaxis are largely mediated by the purinergic Gi-protein coupled receptor P2Y12 and ion channels receptors P2X4 and P2X7 (Davalos et al., 2005; Haynes et al., 2006; Ohsawa et al., 2007; Swiatkowski et al., 2016).

Although originally classified as non-excitable cells, microglia exhibit strong electrophysiological stimulus-response features. While correlations between microglia activation and membrane potential are numerous, they have only been described phenomenologically, and it is not well understood whether changes in membrane potential are cause or consequence of microglia activation. Selective investigation of microglia in their native environment is hampered by the fact that identical molecular pathways exist in other

types of glial cells and in neurons (Kouri et al., 1980; Rangaraju et al., 2015; Schilling and Eder, 2015; Wendt et al., 2017). Therefore, pharmacological manipulations are extremely difficult to interpret unless microglia are cultured in isolation. In isolation, however, microglia assume an activated phenotype, making it impossible to investigate the activation process from the resting state. Genetic manipulations have the required cell-type specificity, but knockdown or knockout approaches change the system in a chronic fashion and may trigger the activation of compensatory mechanisms.

Here we adopt an optogenetic approach to investigate context-dependent behavior of microglia. Using a specific Cre-driver line, we express the light-gated cation channel ChETA specifically in microglia. Two-photon time-lapse imaging allowed us to quantify chemotactic responses while manipulating the membrane potential with blue light pulses. We demonstrate that ATP-mediated hyperpolarization is not an epiphenomenon, but causally related to the chemotactic response.

Results

ChETA effectively depolarizes microglia in response to blue light illumination

We achieved visualization of microglia and expression of the light-gated ion channel ChETA by crossing the tamoxifen-inducible microglia-specific Cre-driver line Cx3cr1^{CreERT2} with the conditional R26-CAG-LSL-ChETA mouse line. To visualize microglia in control experiments, we used the conditional reporter line R26-CAG-LSL-tdTomato (Figure 1A, 1B). From those mice and littermate controls lacking ChETA, we prepared organotypic hippocampal slice cultures, a three-dimensional system in which the cellular architecture is well preserved. Application of (Z)-4-hydroxytamoxifen in the culture medium (24 h) activated cre/loxP-system, leading to selective construct expression in the entire microglia population (Figure 1C). Although microglia become activated during the cutting process and assume a morphology similar to pathologically-activated microglia shortly after preparation, they regain their highly ramified resting morphology over 9-12 days *in vitro* (DIV) (Figure 1D-1H). The fraction of microglia in *stratum radiatum* fluctuates between 5-10% of all cells which is comparable to the density we measured *in vivo* (Figure 1I). Furthermore, microglia membrane properties, such as membrane resistance, capacitance and resting potential are identical in organotypic slice cultures and acute slice preparations (Figure 2A, 2B) (Boucsein et al., 2000; Pagani et al., 2015).

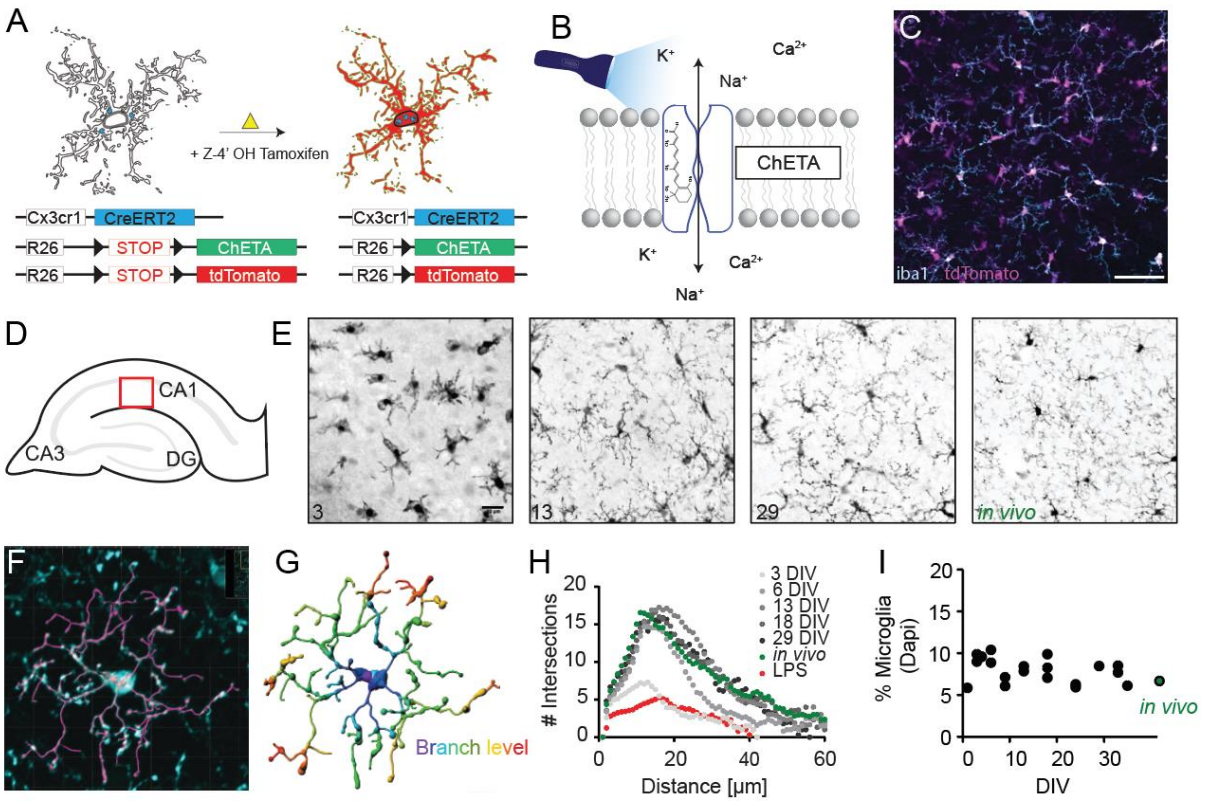

Figure 1 – Microglia specific ChETA expression in organotypic hippocampal slice cultures. (A) Schematic overview of microglia-specific expression. The microglia-driver line Cx3cr1-CreERT2 (blue) is crossed with a reporter mouse line (R26-LSL-tdTomato, red) and the ChETA mouse line (R26-LSL-ChETA, green). After injection of (Z)-4-hydroxytamoxifen the tdTomato and ChETA are expressed in microglia (B) Illustration of the Channelrhodopsin-variant ChETA activated by blue light. Scale bar 25 µm (C) Immunostaining using antibodies against the reporter (tdTomato - red) and microglia (iba1 - cyan). (D) Graphic illustration of the hippocampal structure and the investigated area for microglia morphology in E (red square). (E) Z-projection of confocal images acquired for Sholl analysis of microglia at 3, 13, 29 DIV and in vivo. Scale bar: 25 µm. (F) Confocal image of a microglia in organotypic slice culture. Slice was fixed with PFA and stained against the microglia marker iba1. Overlay with IMARIS analysis (magenta). (G) Result of microglia branch detection with color coding by branching level. (H) Sholl analysis of microglia over time (number of intersections versus distance from cell body). (I) Quantification of % microglia cells between dentate gyrus and CA1 relative to total cell count (DAPI).

Originally, the channelrhodopsin-2 variant ChETA (ChR2/E123T/H134R) was developed for faster response kinetics at the expense of smaller photocurrents (Gunaydin et al., 2010). Therefore, relatively high light intensities and expression levels are required to spike neurons (Berndt et al., 2011). Microglia, however, exhibit an almost 10-times higher input resistance compared to neurons, so small photocurrents generate large changes in microglia membrane potential (Schilling and Eder, 2015). Using increasing blue light intensities, we achieved a maximal depolarization of $\Delta Vm = 36$ mV from microglia resting potential (Figure 2B-2D). During high intensity light pulses, depolarization reached a plateau at 0 mV, the reversal potential of ChR2 (Berndt et al., 2011). Even prolonged repetitive depolarization using light flashes at 1 Hz frequency did not lead to desensitization, but produced photocurrents of constant amplitude (Figure 2E, 2F). In summary, our genetic approach guarantees specific expression of the channelrhodopsin variant ChETA exclusively in microglia and allows rapid light-controlled depolarization in a dose-dependent and cell-type specific fashion.

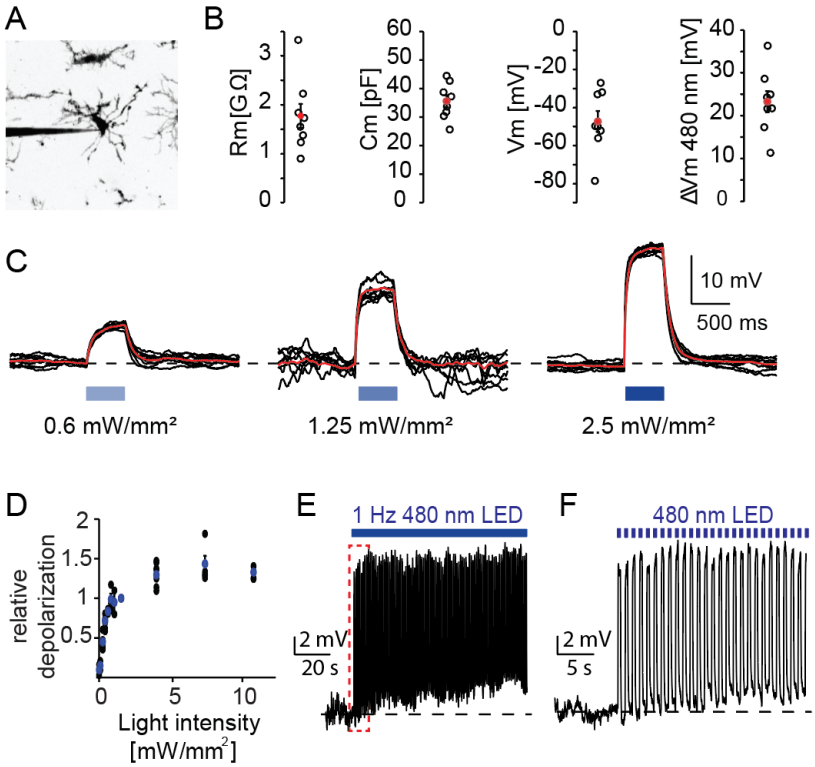

Figure 2 – Optogenetic microglia depolarization using the Channelrhodopsin variant ChETA. (A) Two-photon maximum projection of a microglia patched in organotypic slice culture. Color inversion for better visibility. (B) Microglia cell properties; from left to right: Membrane resistance, cell capacitance, membrane potential, change in membrane potential upon illumination with 1 mW/mm^2 480 nm light. (n=9 microglia, 5 slices) (C) Light-induced membrane depolarizations in microglia. Black: individual sweeps (n=17 sweeps), red: peristimulus time histogram (PSTH) of seven consecutive sweeps with the same light intensity. (D) Relative depolarization of microglia membrane potential 480 nm light. (E) Voltage-clamp recording of a microglia cell with repetitive 1 Hz 480 nm light stimulation at 1 mW/mm^2 (n=7 microglia, 3 slices) (F) Enlargement of red dotted box in E.

Optogenetic depolarization of microglial membrane potential mildly affects microglia morphology and baseline surveillance

Resting microglia constantly monitor their surrounding parenchyma and the surveyed area greatly depends on their morphology. In the resting state, microglia scan larger areas due to the higher number and greater length of processes compared to pathologically activated microglia (Raivich et al., 1999; Streit et al., 1999). The morphological change during pathological activation is often accompanied by strong changes in microglia membrane potential (Eder et al., 1995; Izquierdo et al., 2019; Nguyen et al., 2017a; Visentin et al., 2001). Thus, a direct link between morphology and membrane potential is plausible. Consistent with this, Madry *et al*. found that pharmacological block of the constitutively open outward-rectifying THIK-1 potassium channel, or genetic knock-out thereof, leads to a more depolarized membrane potential in microglia and a more activated morphological phenotype with reduced surveillance (Madry et al., 2018). To investigate whether microglia depolarization by itself causes motility changes, we optically modulated the membrane potential while tracking microglia motility over 50 minutes with two-photon microscopy. After recording baseline motility for 10 minutes, we started optogenetic depolarization for a total duration of 20 minutes using 480 nm light flashes repeated at 1 Hz. Interestingly, optogenetic microglia depolarization did not induce any morphological changes (Fig. 3A, B) and had only minor, transient effects on baseline motility (Fig. 3C) compared to microglia in control slices that did not express ChETA (Fig. 3D). Taken

together, our data show that strong short-term depolarization of microglia membrane potential does not induce any lasting changes in morphology or surveillance behavior.

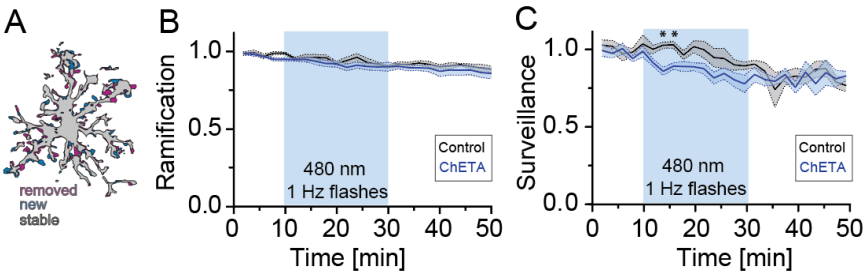

D

Ramification	control	ChETA
0-10 min	0.99±0.00	0.97±0.01
10-20 min	0.95±0.01	0.94±0.01
Surveillance		
0-10 min	1.00±0.01	0.97±0.01
10-20 min	1.01±0.01	0.89±0.01

Figure 3 – Optogenetic depolarization mildly affects microglia baseline properties. (A) Superimposed images of the same microglia at two timepoints one minute apart showing process movement during surveillance (purple, retracted; blue, extended and gray stable processes). (B-C) Relative microglia ramification (B) and surveillance index (C) over the time course of 50 min (ChETA_480, n=4 microglia in 3 slices, control_480, n=8 microglia in 5 slices). Light application (20 min with 480 nm) was started after 10 min of baseline recording. Statistical analysis: Two-way ANOVA with Bonferroni post-hoc comparison (*$p < 0.05$) (D) Overview table of relative ramification and surveillance indices in the 10 min before light application and the first 10 minutes of light application (Average±SEM).

Optogenetic microglia depolarization decelerates chemotactic response kinetics

Microglia maintain a negative resting potential around -40 mV and rapidly hyperpolarize further when sensing extracellular ATP or other nucleotides. This instantaneous hyperpolarization is mediated via the activation of P2Y12 receptors, which results in opening of THIK-1 channels and occurs simultaneously with the onset of microglia process movement towards the source of ATP (Madry et al., 2018; Swiatkowski et al., 2016). Hyperpolarization could be part of the trigger mechanism for the rapid chemotactic response, or just an epiphenomenon. To find out, we altered microglia membrane potential during the chemotactic response using optogenetic depolarization.

After recording microglia baseline motility for 15 minutes with two-photon microscopy, we induced spatially precise tissue damage in a region surrounded by three or four microglia by parking the IR-laser in the center of the field of view for 1.5 seconds. The distance between microglia process tips and laser damage was 35-50 µm (Figure 4A,4 B). Microglia rapidly responded to the laser damage by extending their processes and within a few minutes, the site of damage was completely surrounded by pseudopodia.

To investigate how effectively optogenetic depolarization reduced ATP-mediated hyperpolarizing currents, we performed whole-cell patch clamp recordings from microglia during laser damage (Figure 4C, 4D). Using 480 nm illumination before and during tissue damage, we were able to substantially reduce the amount of hyperpolarization in microglia (Figure 4D). In addition to light stimulation during laser damage, we illuminated the field of view with 1 Hz flashes at 480 nm between the acquired stacks to depolarize microglia throughout the chemotactic response (Figure 4F insert).

After determining the light intensities and frequencies required to effectively depolarize

microglia, the actual chemotactic experiments were then performed without patch-clamp electrodes. We included two types of control experiments: Microglia expressing only the fluorescent protein (no ChETA) and microglia that expressed ChETA, but were not illuminated. These control groups showed similar response kinetics in response to laser damage, demonstrating that neither ChETA expression nor light application alone had an effect on microglia responsiveness ($T½_{ctrl}$ = 7.7 ± 0.7 min, $slope_{ctrl}$ = -0.075 ± 0.006 min^{-1}; $T½_{ChETA_nolight}$ = 7.3 ± 0.7 min, $slope_{ChETA_nolight}$ = -0.090 ± 0.007 min^{-1}; Fig. 4G, 4H). In contrast, microglia expressing ChETA exhibited significantly slower response kinetics when illuminated compared to both control microglia with light and ChETA expressing microglia without light stimulation ($T½_{ChETA+light}$ = 10.7 ± 0.6 min, $slope_{ChETA+light}$ = -0.050 ± 0.004 min^{-1}, Figure 4G, 4H). Under all conditions, response kinetics did not correlate with either microglia distance from laser damage or temperature, which was tightly controlled during the experiments (Figure S1).

In microglia, an increased frequency of Ca^{2+} transients is correlated with pathophysiological activation and other response properties such as chemotaxis. Processes moving towards a source of extracellular ATP exhibit significantly more Ca^{2+} transients compared to resting microglia or processes that are located away from the tissue damage (Pozner et al., 2015). We hypothesize that microglia response kinetics are partially guided by Ca^{2+} influx into the processes located towards the ATP source. Thus, it is conceivable that optogenetic depolarization slowed down chemotaxis by reducing the driving force for Ca^{2+} influx. To investigate whether response kinetics are dependent on Ca^{2+} entry, we performed a series of chemotactic experiments in nominally Ca2+-free extracellular solution. In Ca2+-free extracellular solution, process extension towards the damaged area was significantly slowed down (ΔT½Ca-free = 3.1 min; Figure S2), with kinetics similar to the responses we recorded during optogenetic depolarization (ΔT½ChETA+light = 3 min).

Together, these data demonstrate that microglia hyperpolarization is an important component of the rapid chemotactic response and suggest that the coupling of membrane potential to process elongation might be mediated by enhanced influx of Ca^{2+} ions. However, the onset of chemotactic responses was not affected, neither in optogenetic depolarization nor in Ca^{2+}-free extracellular solution, indicating that this important cellular function is controlled by multiple pathways that act in parallel, partially redundant fashion. Some of them, e.g. G-protein coupled $P2Y_{12}$ receptors are not at all expected to depend on membrane potential or calcium influx. Thus, controlling the membrane potential of microglia can significantly slow down, but not completely switch off the injury response.

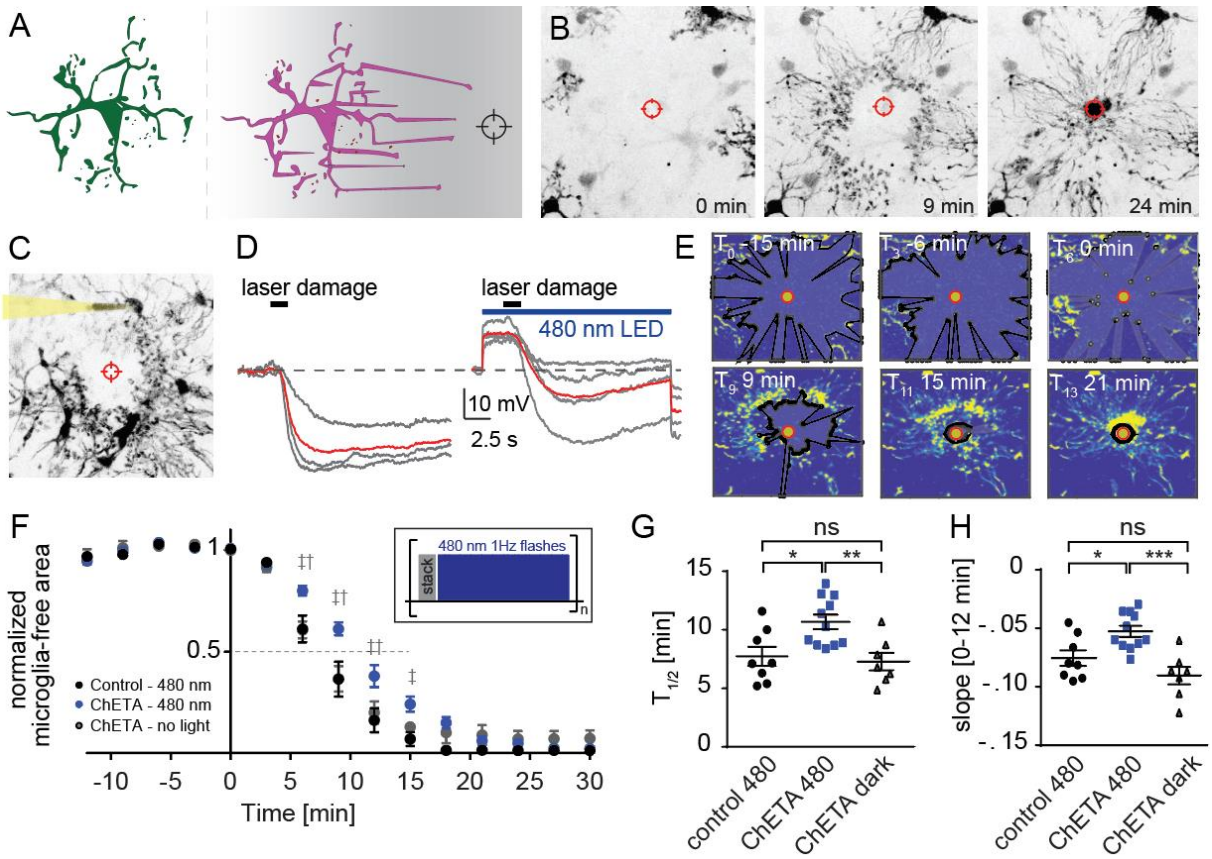

Figure 4 – Optogenetic microglia depolarization decelerates chemotactic response kinetics. (A) Graphic illustration and representative images of microglia chemotaxis towards an induced laser-damage. (B) Two-photon maximum projections of the chemotactic response 0, 9, 24 min after the laser-damage. (C) Two-photon z-projection of a patched microglia during chemotaxis. (D) Voltage-clamp recordings of patched microglia during chemotaxis. Gray: Individual microglial responses from four experiments, red: Average of all experiments. Left: no light stimulation during laser-damage, right: with light stimulation during laser damage. (E) Automated MATLAB analysis of chemotaxis quantified as the reduction in microglia-free area around the laser damage (black polygon) at different time points of the experiment. (F) Relative laser damage response measured as microglia-free area. Black: Control slices (no construct) with light stimulation (n=8 areas, 5 slices). Gray: Experiments with ChETA expression in microglia, but without light stimulation (n=7 areas, 4 slices). Blue: Slices with ChETA expression in microglia combined light stimulation (n=11 areas, 7 slices). Insert: Graphic representation of light stimulation protocol between stack acquisitions. 2-way ANOVA (‡ control480 – ChETA480 $p<0.001$, († ChETA_nolight – ChETA480 $p<0.01$) (G) Summary of 50% response time. (H) Summary microglia-free area slope (0-12 min). In G and H: One-way ANOVA with Tukey's post-hoc comparison (*$p < 0.05$, **$p<0.01$, ***$p<0.001$)

Discussion

Microglia are the only resident immune cells in the brain and although they maintain a negative resting potential and rapidly respond to an external stimulus (ATP) with strong transient hyperpolarization, they are considered non-excitable cells. The classical definition refers to the ability of neurons being able to generate action potentials in response to electrical stimulation. However, many neuronal subtypes never fire action potentials, but respond with graded de- or hyperpolarizing changes in membrane potential (e.g. retinal bipolar cells, photoreceptor cells, most insect neurons), demonstrating that electrical stimulus-response coupling does not require generation of spikes (Barlow, 1953; Baylor and Fuortes, 1970; Werblin and Dowling, 1969). Microglia exhibit reliable changes in membrane potential upon external stimulation, which in turn affect crucial microglia functions such as chemotaxis or phagocytosis (Wu et al., 2007;

Zhao et al., 2018). Here we provide evidence that membrane hyperpolarization is not just a byproduct, but part of the signaling pathway for rapid stimulus-response coupling. As the definition of electrical excitability should be consistent across cell types, we suggest classifying microglia as excitable cells.

Previous studies investigating the depolarizing effect of pharmacological block of K^+ channels on chemotactic response kinetics yielded conflicting results: While K^+ channel block with quinine reportedly abolishes chemotaxis, K^+ channel block with tetrapentylammonium (TPA) did not seem to affect response kinetics (Madry et al., 2018; Wu et al., 2007). It is difficult to determine whether the stimulation strength was comparable in both studies, as chemotaxis was induced by pressure application of ATP at different concentrations and evaluated with different metrics. In both studies, chemotaxis assays were performed in acute brain slices which obviously had sustained severe tissue damage during the slicing process. The state of microglia activation at baseline might therefore depend on subtle details of the slice-making and incubation procedure, leading to poor reproducibility across labs. Microglia in mature organotypic cultures may provide a more stable baseline for chemotaxis and other assays. In addition, our optogenetic approach reduces the risk of unspecific side effects that is the bane of pharmacology. Madry et al. also generated THIK-1 knock-out mice in which microglia are chronically depolarized and show no ATP-induced currents. The chemotactic response was not tested in these animals, but THIK-1-KO microglia had fewer and less motile processes at baseline, suggesting microglia activation. As we show here, acute optogenetic depolarization does not change the morphology and hardly affects surveillance activity of microglia. Thus, it is likely that chronic depolarization triggers changes in expression profile, e.g. downregulation of P2Y12 and upregulation of A2A receptor expression (Orr et al., 2009). While P2Y12 receptors are responsible for the chemotactic response, A2A receptors mediate process retraction from ATP in activated microglia (Madry et al., 2018; Orr et al., 2009).

Ca^{2+} signaling is known to play a key role in microglia activation. The main entry route is not via voltage-gated Ca^{2+} channels, which are only expressed under pathological conditions (Eder, 1998; Espinosa-Parrilla et al., 2015; Saegusa and Tanabe, 2014), but through ligand-gated receptors with high Ca^{2+} permeability. Thus, in contrast to neurons, depolarization reduces Ca^{2+} influx in microglia. A direct link between hyperpolarization and Ca^{2+} signaling has been demonstrated in many types of immune cells and is strengthened by the finding that under resting conditions, microglia exhibit almost no Ca^{2+} transients (4% of resting microglia show a spontaneous Ca^{2+} transient during a 20 min recording session (Pozner et al., 2015)). Pathological hyperpolarization strongly affects microglia function and is accompanied by an

increased number and intensity of Ca^{2+} transients (Brawek et al., 2017; Eichhoff et al., 2011). In particular, potassium channel expression plays an important role in the regulation of the hyperpolarized membrane potential (for review see (Madry and Attwell, 2015; Nguyen et al., 2017b; Thei et al., 2018)). In addition, it was shown that chemotactic responses are accompanied by local Ca^{2+} transients in processes approaching the source of ATP. Thus, optogenetic depolarization might effectively decrease Ca^{2+} currents through ligand-gated receptors, thereby decelerating chemotactic responses. Corroborating evidence comes from our chemotaxis experiments in Ca^{2+}-free saline which phenocopied the effect of optogenetic depolarization. Actin polymerization, one of the major driving forces for pseudopod extension during chemotaxis, is highly regulated by Ca^{2+}-activated enzymes. In our optogenetic depolarization experiments, we were only able to slow down process extension and not completely prevent all movements, which might be due to our pulsed light protocol in combination with a fast closing opsin. However, as the reversal potential for Ca^{2+} is far above the reversal potential of ChETA (-5 mV), even constant illumination would not prevent Ca^{2+} influx completely. The remaining slowed down chemotactic response may therefore be driven by residual calcium influx or by parallel, Ca^{2+}-independent signaling pathways.

In summary, we have shown that ATP-mediated hyperpolarization is not just an epiphenomenon of microglia activation, but rather that it is essential for rapid microglia process extension towards sources of ATP. Microglia could therefore be considered as excitable cells, but they react in an inverted fashion when compared to neurons: Depolarization dampens their reactivity while hyperpolarization is part of their active response to extracellular danger signals. Beyond chemotaxis, optogenetic control of microglia membrane potential opens the possibility to investigate other physiological processes that may depend on membrane potential, such as cytokine release via exosomes, without affecting other cell types.

Methods

Mouse slice culture

Mice carrying a tamoxifen-inducible Cre-recombinase in microglia and the floxed fluorescent marker TdTomato (B6.129; B6.129 - Cx3cr1$^{tm2.1(cre/ERT2)Jung}$ Gt(ROSA26)Sortm$^{9(CAG\text{-}tdTomato)Hze}$) (JAX 020940; JAX 007909) were crossed with mice heterozygously carrying the Gt(ROSA26)Sor$^{tm1(CAG\text{-}COP4*E123T*H134R,\text{-}tdTomato)Gfng}$ (JAX 017455) allele to generate mice expressing ChETA and TdTomato in microglia and littermate controls without ChETA expression in microglia. Hippocampal slice cultures from sex-matched ChETA-expressing mice and littermate controls of were prepared at postnatal day 4–7 as described (Gee et al., 2017). Briefly, mice were anesthetized with 80% CO_2 20% O_2 and decapitated. Hippocampi were dissected in cold slice culture dissection medium containing (in mM): 248 sucrose,

26 $NaHCO_3$, 10 glucose, 4 KCl, 5 $MgCl_2$, 1 $CaCl_2$, 2 kynurenic acid and 0.001% phenol red. pH was 7.4, osmolarity 310-320 mOsm kg^{-1}, and solution was saturated with 95% O_2, 5% CO_2. Tissue was cut into 410 µM thick sections on a tissue chopper and cultured at the medium/air interface on membranes (Millipore PICMORG50) at 37° C in 5% CO_2. For the first 24 h of incubation, 1 µM (Z)-4-hydroxytamoxifen (Sigma H7904) was added to the slice culture medium to induce Cre-activation. No antibiotics were added, and slice culture medium was partially exchanged (60-70%) twice per week and contained (for 500 ml): 394 ml Minimal Essential Medium (Sigma M7278), 100 ml heat inactivated donor horse serum (Sigma H1138), 1 mM L-glutamine (Gibco 25030-024), 0.01 mg ml^{-1} insulin (Sigma I6634), 1.45 ml 5M NaCl (Sigma S5150), 2 mM $MgSO_4$ (Fluka 63126), 1.44 mM $CaCl_2$ (Fluka 21114), 0.00125% ascorbic acid (Fluka 11140), 13 mM D-glucose (Fluka 49152). Slice cultures were used for experiments between 12 and 28 days *in vitro*.

Mice were housed and bred at the University Medical Center Hamburg-Eppendorf. All procedures were performed in compliance with German law and the guidelines of Directive 2010/63/EU.

Mouse genotyping

Tail biopsies were taken from mice at postnatal day 3-4 and lysed using 75 µl alkali buffer containing (in mM): 25 NaOH, 0.2 Na_2-EDTA*$2H_2O$ for 60 min at 95°C and then neutralized using 75 µl 40 mM Tris-HCl. PCR-based genotyping of the Rosa26 locus was performed using the primer combinations 5'-AAGGGAGCTGCAGTGGAGTA-3' and 5'-CCGAAAATCTGTGGGAAGTC-3' for WT and 5'-GGCATTAAAGCAGCGTATCC-3' and 5'-CTGTTCCTGTACGGCATGG-3' for *knock-in* alleles.

Perfusion of animals and preparation of slices

Mice were transcardially perfused with cold phosphate-buffered saline (PBS, pH 7.4), followed by 4% paraformaldehyde in PBS under ketamine (130 mg/kg, WDT) and xylazine (10 mg/kg, WDT) anesthesia. Brains were extracted and post-fixed for 24 h in 4% PFA in 4% paraformaldehyde for 24 h at 4ºC. Before slicing, the tissue was changed to 1x PBS for 20 minutes, then slices of 40 µm were sectioned using Leica vibratome, collected and stored in PBS.

Immunohistochemistry

Organotypic slice cultures were fixed in 4% paraformaldehyde in PBS for 45 min at room temperature and stored in PBS at 4 ºC until further use. Fixed cultures or brain slices from perfused animals were blocked for 2 hours at room temperature using goat-serum based blocking solution containing (in %): 10 Goat serum (Capricorn), 0.2 Bovine Serum Albumin (Sigma-Aldrich A2153-10G), 0.5 TritonX-100 (Sigma Aldrich T-9284). Primary antibodies were directed against IBA1 (rabbit-anti-iba1 WAKO chemicals 019-19741 1:1000) and TdTomato (mouse-anti-dsRed Takara 632392 1:1000). Secondary antibodies were goat anti-rabbit or anti-mouse conjugated with Alexa dyes 488 and 568 (1:1000), respectively (Life Technologies A11008 and A11004). Antibodies were prepared in carrier solution containing (in %): 1 Goat serum (Capricorn), 0.2 Bovine Serum Albumin (Sigma-Aldrich A2153-10G), 0.3 TritonX-100 (Sigma Aldrich T-9284). Primary antibodies were applied overnight at 4 ºC; before application of secondary antibodies, slices were washed three times 10 min with PBS and then incubated

with secondary antibodies for 2 hours at room temperature. Slices were washed for three times with PBS, incubated with DAPI (Molecular Probes, Invitrogen) for 5 min and then mounted (Thermo Scientific 9990402). Slices were imaged using an Olympus FV-1000 confocal microscope and microglia morphology and cell count was analyzed using the Imaris Software (Bitplane).

Two photon imaging and microglia patch clamp

Organotypic hippocampal slice cultures were placed in the recording chamber of a custom-built two-photon laser scanning microscope based on an Olympus BX51WI microscope with a pE-4000 LED light source for epifluorescence and activation of ChETA. The LED light source was controlled using a TTL trigger input. Power density of the 470 nm light was measured using a digital optical power and energy meter console with an attached photodiode power sensor (Thorlabs).

The microscope was equipped with a WPlan-Apochromat 40× 1.0 NA (Zeiss) or HC Fluotar L 25x 0.95 NA (Leica) objective and controlled by ScanImage 2017b (Vidrio). A pulsed Ti:Sapphire laser (Chameleon Ultra, Coherent) controlled by an electro-optic modulator (350-80, Conoptics) was used to image microglia with 1040 nm. Z-stacks were acquired with step intervals between 2 and 3 µm.

The slices were continuously perfused with either an artificial cerebrospinal fluid (ACSF) saturated with 95% O_2 and 5% CO_2 consisting of (in mM): 119 NaCl, 26.2 $NaHCO_3$, 11 D-glucose, 1 NaH_2PO_4, 2.5 KCl, 4 $CaCl_2$, 4 $MgCl_2$. (pH 7.4, 308 mOsm) at 27-29° C or with a HEPES-buffered solution (in mM): 135 NaCl, 2.5 KCl, 10 Na-HEPES, 12.5 D-glucose, 1.25 NaH_2PO_4, 2 $CaCl_2$, 1 $MgCl_2$ (pH 7.4). Nominally Ca^{2+}-free extracellular solution consisted of (in mM): 135 NaCl, 2.5 KCl, 10 Na-HEPES, 12.5 D-glucose, 1.25 NaH_2PO_4, 3 $MgCl_2$ (pH 7.4).

Whole-cell recordings from microglia in stratum radiatum were made with patch pipettes (6–8 MΩ) filled with (in mM): 135 K-gluconate, 4 $MgCl_2$, 4 Na_2-ATP, 0.4 Na-GTP, 10 Na_2-phosphocreatine, 3 sodium-L-ascorbate, and 10 HEPES (pH 7.2, 295 mOsm kg^{-1}).

Fluorescence guided microglia whole-cell patch clamp recordings were done using a Multiclamp 700B amplifier (Molecular Devices) under the control of Ephus software written in Matlab (The MathWorks) (Suter et al., 2010). Series resistance was below 20 MΩ. Z-stacks of patch-clamped microglia were acquired to document their morphology.

The tissue damage was performed in a standardized fashion in a region between three to four microglia at a distance of approximately 35-50 µm by parking the IR-laser in the center of the imaged region.

Image analysis of microglia baseline surveillance and chemotaxis

Microglial baseline surveillance. We combined several analysis steps into a semi-automated workflow. Image data were background subtracted (rolling ball radius = 30 pixels) and median filtered (radius = 1 pixel) with ImageJ. In order to correct for small positional shifts that occurred during acquisition, we registered all images from a time-lapse recording to the first image of the series (Efficient subpixel image registration by cross-correlation, version 1.1, MATLAB Central File Exchange). Images were then binarized using Otsu's method (threshold set to 50% calculated value). Based on a maximum projection of both images and binary images, a mask was drawn to define the region considered for

motility analysis. Within the masked region we counted the number of pixels that remained stable, that were lost, and that were gained throughout the time series. From the covered areas and perimeters we calculated ramification and surveillance indices.

Microglial response to laser-induced tissue damage. We created a semi-automated workflow (Matlab code, release R2016b, MathWorks®, github if required) to analyse microglial responses to laser-induced tissue damage. Individual images from a time-lapse series (2D, Number, time step) were median filtered (3x3 kernel size), converted to binary form (Otsu's method), polished using dilation, erosion steps and filling of holes. A spot (eccentricity < 0.5, size > 50 pixel) near the image centre was defined as the site at which tissue damage was initiated. The image from the tissue damage time point with detected spot coordinates was presented to the user for visual inspection; the location of the spot was corrected if necessary. For further processing, images prior to the damage time point were averaged (median pixel values) to obtain a background image from which an intensity threshold was calculated (locally adaptive threshold, specificity = 0.5). All images were then background subtracted and binarized using the intensity threshold. The region around the damage centre (spot dilated with a 9x9 disc) was masked and objects smaller than 5 pixels were removed. Following polishing using a dilation/erosion (5x5 kernel), step object areas, distances, and positions relative to the damage centre sectioned into 36 radial slices were extracted.

Acknowledgements

We thank M. Fuhrmann for providing us with two male mice of the Jackson Laboratory (JAX) mouse lines JAX 020940 and JAX 007909. We thank I. Hanganu-Opatz for providing us with a breeding pair of the JAX mouse line 017455. We thank I. Ohmert and S. Graf for the preparation of organotypic cultures and excellent technical assistance. This study was supported by the State Excellence Initiative Hamburg (LFF) and German Research Foundation (DFG) grants FOR 2419 278170285, SPP 1665 220176618 and SFB 936 178316478.

Contributions

L.L. and T.G.O. designed the experiments and prepared the manuscript. L.L. performed microglia patch clamp recordings, microglia chemotaxis and motility experiments, immunohistochemical experiments and all data analysis. M-L.B. performed microglia motility experiments and immunohistochemical experiments. C.S. wrote software to analyze microglia motility and chemotaxis.

References

Barlow, H.B. (1953). Summation and inhibition in the frog's retina. J. Physiol. *119*, 69–88.

Baylor, D.A., and Fuortes, M.G.F. (1970). Electrical responses of single cones in the retina of the turtle. J. Physiol. *207*, 77–92.

Berndt, A., Schoenenberger, P., Mattis, J., Tye, K.M., Deisseroth, K., Hegemann, P., and Oertner, T.G. (2011). High-efficiency channelrhodopsins for fast neuronal stimulation at low light levels. Proc. Natl. Acad. Sci. U. S. A. *108*, 7595–7600.

Boucsein, C., Kettenmann, H., and Nolte, C. (2000). Electrophysiological properties of microglial cells in normal and pathologic rat brain slices. Eur. J. Neurosci. *12*, 2049–2058.

Brawek, B., Liang, Y., Savitska, D., Li, K., Fomin-Thunemann, N., Kovalchuk, Y., Zirdum, E., Jakobsson, J., and Garaschuk, O. (2017). A new approach for ratiometric in vivo calcium imaging of microglia. Sci. Rep. *7*, 6030.

Davalos, D., Grutzendler, J., Yang, G., Kim, J.V., Zuo, Y., Jung, S., Littman, D.R., Dustin, M.L., and Gan, W.-B. (2005). ATP mediates rapid microglial response to local brain injury in vivo. Nat. Neurosci. *8*, 752–758.

Eder, C. (1998). Ion channels in microglia (brain macrophages). Am. J. Physiol. *275*, C327–C342.

Eder, C. (2005). Regulation of microglial behavior by ion channel activity. J. Neurosci. Res. *81*, 314–321.

Eder, C., Fischer, H.G., Hadding, U., and Heinemann, U. (1995). Properties of voltage-gated potassium currents of microglia differentiated with granulocyte/macrophage colony-stimulating factor. J. Membr. Biol. *147*, 137–146.

Eichhoff, G., Brawek, B., and Garaschuk, O. (2011). Microglial calcium signal acts as a rapid sensor of single neuron damage in vivo. Biochimica et Biophysica Acta - Molecular Cell Research *1813*, 1014–1024.

Espinosa-Parrilla, J.F., Martínez-Moreno, M., Gasull, X., Mahy, N., and Rodríguez, M.J. (2015). The L-type voltage-gated calcium channel modulates microglial pro-inflammatory activity. Mol. Cell. Neurosci. *64*, 104–115.

Gee, C.E., Ohmert, I., Wiegert, J.S., and Oertner, T.G. (2017). Preparation of Slice Cultures from Rodent Hippocampus. Cold Spring Harb. Protoc. *2017*.

Gunaydin, L.A., Yizhar, O., Berndt, A., Sohal, V.S., Deisseroth, K., and Hegemann, P. (2010). Ultrafast optogenetic control. Nat. Neurosci. *13*, 387–392.

Haynes, S.E., Hollopeter, G., Yang, G., Kurpius, D., Dailey, M.E., Gan, W.-B., and Julius, D. (2006). The P2Y12 receptor regulates microglial activation by extracellular nucleotides. Nat. Neurosci. *9*, 1512–1519.

Ince, C., Coremans &Ypey, J.M.C.C.D.L., Leijh, P.C.J., Verveen, A.A., and Van Furth, R. (1988). Phagocytosis by human macrophages is accompanied by changes in ionic channel currents. J. Cell Biol. *106*, 1873–1878.

Izquierdo, P., Attwell, D., and Madry, C. (2019). Ion Channels and Receptors as Determinants of Microglial Function. Trends Neurosci. *42*, 278–292.

Kouri, J., Noa, M., Diaz, B., and Niubo, E. (1980). Hyperpolarisation of rat peritoneal macrophages phagocytosing latex particles. Nature *283*, 868–869.

Lee, J.E., Liang, K.J., Fariss, R.N., and Wong, W.T. (2008). Ex Vivo Dynamic Imaging of Retinal Microglia Using Time-Lapse Confocal Microscopy. Invest. Ophthalmol. Vis. Sci. *49*, 4169–4176.

Madry, C., and Attwell, D. (2015). Receptors, Ion Channels, and Signaling Mechanisms Underlying Microglial Dynamics. J. Biol. Chem. *290*, 12443–12450.

Madry, C., Kyrargyri, V., Arancibia-Cárcamo, I.L., Jolivet, R., Kohsaka, S., Bryan, R.M., and Attwell, D. (2018). Microglial Ramification, Surveillance, and Interleukin-1β Release Are Regulated by the Two-Pore Domain K+ Channel THIK-1. Neuron *97*, 299–312.e6.

Newell, E.W., and Schlichter, L.C. (2005). Integration of K + and Cl-currents regulate steady-state and dynamic membrane potentials in cultured rat microglia. J. Physiol. *567*, 869–890.

Nguyen, H.M., Grössinger, E.M., Horiuchi, M., Davis, K.W., Jin, L.-W., Maezawa, I., and Wulff, H. (2017a). Differential Kv1.3, KCa3.1, and Kir2.1 expression in "classically" and "alternatively" activated microglia. Glia *65*, 106–121.

Nguyen, H.M., Blomster, L.V., Christophersen, P., and Wulff, H. (2017b). Potassium channel expression and function in microglia: Plasticity and possible species variations. Channels *11*, 305–315.

Nimmerjahn, A. (2005). Resting Microglial Cells Are Highly Dynamic Surveillants of Brain Parenchyma in Vivo. Science *308*, 1314–1318.

Ohsawa, K., Irino, Y., Nakamura, Y., Akazawa, C., Inoue, K., and Kohsaka, S. (2007). Involvement of P2X4 and P2Y12 receptors in ATP-induced microglial chemotaxis. Glia *55*, 604–616.

Orr, A.G., Orr, A.L., Li, X.J., Gross, R.E., and Traynelis, S.F. (2009). Adenosine A2Areceptor mediates microglial process retraction. Nat. Neurosci. *12*, 872–878.

Pagani, F., Paolicelli, R.C., Murana, E., Cortese, B., Angelantonio, S.D., Zurolo, E., Guiducci, E., Ferreira, T.A., Garofalo, S., Catalano, M., et al. (2015). Defective microglial development in the hippocampus of Cx3cr1 deficient mice. Front. Cell. Neurosci. *09*, 111.

Paolicelli, R.C., Bolasco, G., Pagani, F., Maggi, L., Scianni, M., Panzanelli, P., Giustetto, M., Ferreira, T.A., Guiducci, E., Dumas, L., et al. (2011). Synaptic pruning by microglia is necessary for normal brain development. Science *333*, 1456–1458.

Pozner, A., Xu, B., Palumbos, S., Gee, J.M., Tvrdik, P., and Capecchi, M.R. (2015). Intracellular calcium dynamics in cortical microglia responding to focal laser injury in the PC::G5-tdT reporter mouse. Front. Mol. Neurosci. *8*, 12.

Raivich, G., Bohatschek, M., Kloss, C.U.A., Werner, A., Jones, L.L., and Kreutzberg, G.W. (1999). Neuroglial activation repertoire in the injured brain: Graded response, molecular mechanisms and cues to physiological function. Brain Research Reviews *30*, 77–105.

Rangaraju, S., Gearing, M., Jin, L.-W., and Levey, A. (2015). Potassium channel Kv1.3 is highly expressed by microglia in human Alzheimer's disease. J. Alzheimers. Dis. *44*, 797–808.

Saegusa, H., and Tanabe, T. (2014). N-type voltage-dependent Ca2+ channel in non-excitable microglial cells in mice is involved in the pathophysiology of neuropathic pain. Biochem. Biophys. Res. Commun. *450*, 142–147.

Schilling, T., and Eder, C. (2015). Microglial K+channel expression in young adult and aged mice. Glia *63*, 664–672.

Streit, W.J., Walter, S.A., and Pennell, N.A. (1999). Reactive microgliosis. Progress in Neurobiology *57*, 563–581.

Suter, B.A., O'Connor, T., Iyer, V., Petreanu, L.T., Hooks, B.M., Kiritani, T., Svoboda, K., and Shepherd, G.M.G. (2010). Ephus: multipurpose data acquisition software for neuroscience experiments. Front. Neural Circuits *4*, 100.

Swiatkowski, P., Murugan, M., Eyo, U.B., Wang, Y., Rangaraju, S., Oh, S.B., and Wu, L.-J. (2016). Activation of microglial P2Y12 receptor is required for outward potassium currents in response to neuronal injury. Neuroscience *318*, 22–33.

Thei, L., Imm, J., Kaisis, E., Dallas, M.L., and Kerrigan, T.L. (2018). Microglia in Alzheimer's Disease: A Role for Ion Channels. Front. Neurosci. *12*.

Visentin, S., Renzi, M., and Levi, G. (2001). Altered outward-rectifying K+ current reveals microglial activation induced by HIV-1 Tat protein. Glia *33*, 181–190.

Wendt, S., Maricos, M., Vana, N., Meyer, N., Guneykaya, D., Semtner, M., and Kettenmann, H. (2017). Changes in phagocytosis and potassium channel activity in microglia of 5xFAD mice indicate alterations in purinergic signaling in a mouse model of Alzheimer's disease. Neurobiol. Aging *58*, 41–53.

Werblin, F.S., and Dowling, J.E. (1969). Organization of the retina of the mudpuppy, Necturus maculosus. II. Intracellular recording. J. Neurophysiol. *32*, 339–355.

Wu, L.-J., Vadakkan, K.I., and Zhuo, M. (2007). ATP-induced chemotaxis of microglial processes requires P2Y receptor-activated initiation of outward potassium currents. Glia *55*, 810–821.

Zhao, Y., Wu, X., Li, X., Jiang, L.-L., Gui, X., Liu, Y., Sun, Y., Zhu, B., Piña-Crespo, J.C., Zhang, M., et al. (2018). TREM2 Is a Receptor for β-Amyloid that Mediates Microglial Function. Neuron *97*, 1023–1031.e7.